Structure and magnetic properties of nonsuperconducting doped Co and Fe $Bi_2Sr_2Cu_{1-x}M_xO_y$ phases

J. M. Tarascon, P. F. Miceli, P. Barboux, D. M. Hwang, G. W. Hull, M. Giroud, and L. H. Greene
Bell Communications Research, Red Bank, New Jersey 07701

Yvon LePage, W. R. McKinnon, E. Tselepis, and G. Pleizier
National Research Council of Canada, Ottawa, Canada K1A OR9

M. Eibschutz
AT&T Bell Laboratories, Murray Hill, New Jersey 07974

D. A. Neumann and J. J. Rhyne
National Institute of Standards and Technology, Gaithersburg, Maryland 20899
(Received 24 January 1989)

The structure and magnetic properties of the $Bi_2Sr_2Cu_{1-x}M_xO_y$ (M=Co and Fe) materials were studied. The limits of solid solution formation are at $x=0.5$ for the Fe system and $x=1$ for the Co system. Crystals of the new $Bi_2Sr_2CoO_y$ phase were grown and the structure established by x-ray crystallography. The subcell is the same as that of the 10-K superconductor, $Bi_2Sr_2CuO_y$, but the superstructure is different, as it exhibits a commensurate modulation of periodicity 4 instead of 5. Extra oxygen is accommodated in the Bi layers, as in $Bi_2Sr_3Fe_2O_y$, and the structure of the Bi-O layers can be described as 50% rocksalt type and 50% oxygen-deficient perovskite for $x=1$, but with disorder at the oxygen positions. The formal valence of Co in this compound is about 2.5 ± 0.2 as deduced from structural and chemical measurements, whereas Fe adopts the oxidation state +3 as deduced by Mössbauer measurements. $Bi_2Sr_2CoO_y$ is an antiferromagnetic insulator with the spins lying within the CoO_2 sheets and the antiferromagnetic ordering temperature (T_N) is sensitive to processing conditions and composition changes. The high anisotropy of the susceptibility suggests that $Bi_2Sr_2CoO_y$ may be an Ising or XY antiferromagnet.

INTRODUCTION

Magnetic impurities in conventional superconductors strongly depress the superconducting transition temperature T_c. But in the new high-T_c cuprates La_2CuO_4 and $YBa_2Cu_3O_y$, in which superconductivity is believed to be confined within CuO_2 planes, T_c is depressed whether Cu is replaced by magnetic or diamagnetic ions.[1-3] For $YBa_2Cu_3O_y$, however, the study of this depression of T_c is complicated because there are two different copper sites that the impurity can occupy, as opposed to La_2CuO_4, where there is only one. The Bi-based high-T_c materials of general formula $Bi_2Sr_2Ca_{n-1}Cu_nO_y$ with $n=1$, 2, and 3, where all the Cu atoms lie in CuO_2 planes,[4] is another simpler system for studying the effect of magnetic impurities.

All of the Bi-based superconductors have an incommensurate structural modulation.[5] We recently discussed the crystal chemistry of this modulation within the 80-K superconductor $Bi_2Sr_2CaCu_2O_{8+y}$ ($n=2$) in a study of the isostructural commensurate $Bi_{10}Sr_{15}Fe_{10}O_{46}$ phase.[6] This study showed that the modulation is caused by the insertion of extra oxygen in a perovskite position within the Bi layers. The $Bi_2Sr_2CuO_y$ phase ($n=1$), whose basic unit cell has been found to be either orthorhombic[7] or face-centered monoclinic,[8] has a commensurate modulation of the structure,[8] and it is likely that the modulation has the same origin in all the Bi phases, but the structures of the various compounds must be solved to verify this hypothesis.

We have previously shown that Co and Fe can be substituted for Cu in the $Bi_2Sr_2CuO_y$ phase.[9] To address the above questions of structural modulation and magnetism, we have studied these substitutions on the Cu sites in more detail. We have followed the evolution of magnetism and the structural modulation as a function of the amount of Cu replaced by Fe and Co. During this work, we synthesized a structurally related Bi phase containing only Co ($Bi_2Sr_2CoO_y$), in both bulk or single-crystal form, and solved its structure. We present both the structure and the magnetic properties. We find that within this phase the structural modulation is commensurate, and that the magnetic properties suggest hidden ferromagnetism, similar to that found in La_2CuO_4 but with the canted component of the spins lying in the CoO_2 planes.

SYNTHESIS

Samples of nominal composition $Bi_2Sr_2Cu_{1-x}M_xO_y$ (M=Co and Fe) were prepared by thoroughly mixing appropriate amounts of the starting oxides and carbonates, then heating the mixture in air for 24 h at temperatures ranging from 860–900 °C and 900–950 °C when M=Co and Fe, respectively. Higher temperatures are required for samples with increased doping content x. The reacted

powders were then pressed into pellets, reannealed in air at the above temperatures for 24 h, and rapidly cooled (at 10°/min) to room temperature.

X-ray studies of the resulting samples summarized in Table I show that for M =Co, single-phase materials are obtained for all x. With M =Fe the materials are multiphase for x greater than 0.6. The subcell parameters are displayed in Fig. 1 as a function of x for the $Bi_2Sr_2Cu_{1-x}M_xO_y$ series. The most prominent feature is the sharp drop in the subcell volume at $x=0.5$ and $x=0.25$ for the Co and Fe series, respectively, which might indicate subtle structural changes. The powder patterns for samples close to the Fe composition, $x=0.25$, show the coexistence of two sets of lines, indicating a noncontinuous structural change. This is in contrast with the Co series where (within the accuracy of the measurements) we did not detect coexistence of two phases for compositions close to $x=0.5$.

The atmosphere used during the processing of $Bi_2Sr_2CoO_y$ is important. When samples are annealed at 840 °C under Ar, the structure is preserved, although the unit-cell volume increases by 1 Å^3. In contrast, when heated in oxygen at 820 °C the material became multiphase as indicated by its x-ray powder diffraction pattern which shows two sets of Bragg peaks with the most intense ones corresponding to the $n=1$ phase. Among the weak extra Bragg peaks, the one at $2\theta=6°$ (for Cu radiation) suggests the existence of another phase (denoted as the $n=2$ phase) which will be discussed elsewhere.[10] This "$n=2$" phase becomes predominant when lower reannealing temperatures (<800 °C) under oxygen are used.

To determine the stability of the $n=1$ phase under higher pressure of oxygen, we performed (as previously reported for the synthesis of pure undoped $Bi_2Sr_2CuO_y$ phase[4]), solid-state reactions within sealed quartz ampoules using strontium peroxide as the source of Sr (to produce a pressure of oxygen). From the volume of the ampoule and the amount of SrO_2, the pressure in the tube was roughly estimated at 20 bars at temperatures of 800 °C. The Fe and Co series were made using this technique at temperatures of 860 °C and 840 °C, respectively. We found that $Bi_2Sr_2Cu_{1-x}Co_xO_y$ single-phase materials can only be obtained up to $x=0.6$. At higher Co concentrations, the material was multiphase containing the $n=1$ phase and a layered phase "$n=2$ or 2:3:0:2" with a c-axis of 29.8 Å. The amount of this layered phase was found to increase with increasing Co content, so that no Bragg peaks corresponding to the $n=1$ phase could be detected in the x-ray powder diffraction pattern of the $x=1$ sample. For the Fe series, a less crucial effect was observed, since a range of solubility was found to exist from 0 to 0.5 ± 0.1 when the materials are prepared using SrO_2 in contrast to 0.6 ± 0.1 when they are prepared in air. At higher Fe concentrations we observed the formation of the $Bi_2Sr_3Fe_2O_{9.2}$ ($n=2$) phase, whose structure has been discussed elsewhere.[6] These experiments demonstrate that the x, T, $P(O_2)$ phase diagram for the stability of the $Bi_2Sr_2CoO_y$ is quite complex because of the $n=2$ phase as the competing phase. The main results are that (1) single-phase $Bi_2Sr_2CoO_y$ materials can be obtained in air at temperatures of 870 ± 30 °C or at lower temperatures in partially reducing ambient and (2) that lowering the synthesis temperature either in air or oxygen, or increasing the oxygen pressure at $T=800$ °C, always result in a multiphase sample. Synthesis under oxygen usually favors the high oxidation state of the metal elements

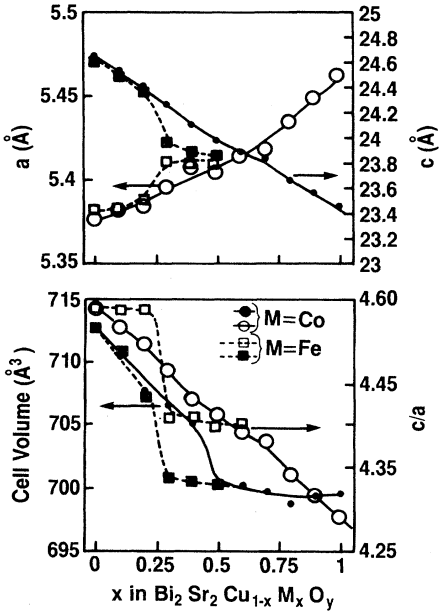

FIG. 1. Subcell parameters (a,c,V) and c/a ratio as a function of the $3d$ metal content in $Bi_2Sr_2Cu_{1-x}M_xO_y$ series (M =Co, Fe). Circles and squares refer to the Co and Fe series, respectively. Open symbols refer to the a and c lattice parameters, whereas solid symbols refer to the cell volume and c/a ratio.

TABLE I. Subcell parameters a, c, and V for the $Bi_2Sr_2Cu_{1-x}M_xO_y$ (M =Fe, Co) series.

x	a (Å)	c (Å)	V (Å)
	M =Co		
0.0	5.376	24.56	712.6
0.1	5.381	24.56	711.1
0.2	5.384	24.41	707.7
0.3	5.393	24.31	707.1
0.4	5.407	24.11	705.0
0.5	5.411	23.99	702.4
0.6	5.417	23.93	701.9
0.7	5.422	23.87	701.8
0.8	5.434	23.67	699.2
0.9	5.450	23.59	700.9
1.0	5.464	23.47	700.7
	M =Fe		
0.1	5.388	24.47	710.5
0.2	5.385	24.47	709.7
0.3	5.423	23.87	702.4
0.4	5.418	23.87	700.9
0.5	5.413	23.87	699.6
$0.5<x<1$		Multiphase	

within a compound. Thus the observation that the 2:2:0:1 is not stable under oxygen for high Co content or even in air for high Fe content, suggests that the 2:2:0:1 phase does not allow an oxidation state of Fe(Co) as great as the 2:3:0:2, as we will confirm shortly.

The oxygen content in this phase was determined directly by thermogravimetric measurements (TGA) as described elsewhere,[11] or indirectly by chemical analysis.[12] In the chemical method, the material is dissolved in an acidified solution and the solution is titrated with a second solution of $Ce(SO_4)_2$ ($10^{-2}N$). Ce^{4+} oxidizes Co^{2+} to Co^{3+}, so the amount of Ce^{4+} consumed gives the formal valence of Co and, thereby, the amount of oxygen, assuming that Bi and Sr have a fixed valence of +3 and +2, respectively. By chemical analysis we found that the formal valence for Co is 2.3 ± 0.1, resulting in an oxygen content of 6.15 ± 0.05 per unit formula. A similar formal valence for Co (within the accuracy of the titration) was found for the material annealed under argon. TGA measurements performed on several powdered samples and on powdered single crystals consistently gave oxygen contents ranging from 6.4 to 6.5. The discrepancy between the chemical analysis and TGA may arise from loss of Bi during the reduction under H_2, because a reddish deposit was observed along the wall of the TGA furnace during the reduction experiment.

With the hope of determining more quantitatively how the $n=1$ Co phase is affected by ambient, several TGA (weight-loss measurements) were performed with identical results. A TGA trace is reported in the inset of Fig. 8 for the $Bi_2Sr_2CoO_y$ phase heated in argon, cooled in argon, and then reheated in air. Note that up to temperatures of 500 °C the weight loss (0.15%) of the sample heated under argon is equal to its weight gain (0.15%) when reheated under air, indicating a reversible intercalation of 0.06 oxygen atoms per formula unit. At higher temperatures the weight gain becomes smaller than the weight loss, most likely due to a loss of Bi, which is quite volatile at high temperatures, and especially so under vacuum. Thus, with respect to its oxygen affinity this compound bears a striking similarity to $Bi_2Sr_2CaCu_2O_y$ and La_2CuO_y for which a small range of oxygen nonstoichiometry ($\Delta y = 0.04$) was found.[13,14]

Crystals of the $Bi_2Sr_2CoO_y$ phase (either in platelet or needlelike form) were prepared in a dense alumina crucible ($\frac{1}{2}$ in. diam and 2 in. high) containing an 11 g charge composed of 60% Bi_2O_3, 31% $SrCO_3$, and 9% Co_3O_4 by weight. The charge was heated in air to 1000 °C over a period of 6 h, maintained at this temperature for 2 h, slowly cooled to 700 °C at a rate of 6 °C per h, and then removed from the furnace at this temperature. This treatment partially melted the material. Within the charge were large cavities containing free crystals (sizes ranging from several micrometers to 3 or 4 mm) that were used for the structural and physical measurements reported herein.

STRUCTURE

An 8-μm-thick platelet with metallic luster and specular reflection was selected and turned out to be an orthorhombic crystal with space group *I2mb* and cell parameters $a = 21.836(5)$, $b = 5.4615(8)$, $c = 23.450(4)$ Å. The plane of the platelet was (002).

The essential details of the structure data collection and data reduction are given in Table II. Direct methods followed by least-squares refinement and difference-Fourier maps gave the atomic positions in Table III. The resulting metal positions are schematically shown in Fig. 2. For the $Bi_8Sr_8Co_4O_{25}$ phase [or 2:2:0:1 (Co), for short], the modulation along the *a*-axis is a fourfold multiplication of the subcell parameter. In previously studied compounds, the modulation was fivefold, in $Bi_2Sr_2CuO_y$ [2:2:0:1 (Cu)] (Ref. 8) and $Bi_2Sr_3Fe_2O_y$ [2:3:0:2 (Fe)] (Ref. 6), or approximately fivefold, in $Bi_2Sr_2CaCu_2O_y$ [2:2:1:2 (Cu)].[15] The superstructure of the 2:2:0:1 (Co) resembles those of 2:3:0:2 (Fe) or 2:2:1:2 (Cu) phases more closely than it resembles that of its Cu analog, 2:2:0:1 (Cu). The structure of the Sr-Co-Sr layers is distorted perovskite, with all oxygen atoms present [contrary to the work of Onoda and Soto[8] for 2:2:0:1 (Cu)], and the Bi-O layers approximately 50% rocksalt type, 50% perovskite type. The total oxy-

TABLE II. Crystal data, data collection, and refinement.

Formula:	$Bi_8Sr_8Co_4O_{25}$, $Z=4$
Space group:	*I2mb*, No 46 with axes relabeled
Cell parameters (Å):	$a=21.836(5)$, $b=5.4615(8)$, $c=23.450(4)$
Radiation:	Graphite-monochromatized Mo $K\alpha$
Diffractometer:	CAD-4 with NRCCAD[a] control
Reflections measured:	6293
Unique reflections:	2280
Observed (2.5 sigma *I*):	1077
Absorption correction:	Gauss integration
R_{sym}:	4.9%
Independent atoms:	41*B*
Number of parameters:	172
Refinement:	Full matrix on 2280 reflections, unit weights
Refinement on observed reflections:	7.1%

All calculations were performed with the NRCVAX[b] system of programs

[a]Reference 32. [b]Reference 33.

TABLE III. Atomic parameters x, y, z, and B_{iso}. Estimated standard deviations refer to the last digit printed. B_{iso} is the mean of the principle axes of the thermal ellipsoid. OB refers to the oxygen atoms within the Bi-O layer. OS refers to the oxygen atoms within the Sr-O layer. OC refers to the oxygen atoms within the Co-O layer.

Atom	Multiplicity	x	y	z	B_{iso}	Occupation
Bi-1	4	0.0000	$\frac{1}{4}$	0.0742(1)	1.7(1)	
Bi-2	4	0.1111(4)	$\frac{3}{4}$	0.0710(3)	2.1(2)	
Bi-3	4	0.2290(4)	$\frac{1}{4}$	0.0623(3)	2.1(2)	
Bi-4	4	0.3602(8)	$\frac{3}{4}$	0.0546(2)	3.7(3)	
Bi-5	4	0.5002(6)	$\frac{1}{4}$	0.0515(1)	1.6(1)	
Bi-6	4	0.6434(6)	$\frac{3}{4}$	0.0573(2)	2.8(2)	
Bi-7	4	0.7718(4)	$\frac{1}{4}$	0.0649(2)	1.8(2)	
Bi-8	4	0.8883(3)	$\frac{3}{4}$	0.0707(2)	1.5(1)	
Sr-1	4	0.0011(5)	$\frac{3}{4}$	0.1944(3)	1.2(2)	
Sr-2	4	0.1181(5)	$\frac{1}{4}$	0.1886(5)	1.3(3)	
Sr-3	4	0.2385(7)	$\frac{3}{4}$	0.1750(6)	2.0(4)	
Sr-4	4	0.3644(9)	$\frac{1}{4}$	0.1579(8)	3.6(6)	
Sr-5	4	0.5034(2)	$\frac{3}{4}$	0.1503(5)	4.3(6)	
Sr-6	4	0.6366(7)	$\frac{1}{4}$	0.1610(8)	3.1(6)	
Sr-7	4	0.7638(6)	$\frac{3}{4}$	0.1793(7)	3.1(5)	
Sr-8	4	0.8832(6)	$\frac{1}{4}$	0.1906(6)	3.4(5)	
Co-1	4	0.0015(2)	$\frac{1}{4}$	0.2786(5)	1.7(2)	
Co-2	4	0.1294(9)	$\frac{3}{4}$	0.2599(8)	2.2(3)	
Co-3	4	0.2524(7)	$\frac{1}{4}$	0.2392(4)	0.6(2)	
Co-4	4	0.3754(6)	$\frac{3}{4}$	0.2248(5)	0.3(3)	
OB-1	8	−0.010(3)	0.633(2)	0.076(3)	0.8	$\frac{1}{2}$
OB-2	8	0.097(3)	0.355(2)	0.064(3)	0.8	$\frac{1}{2}$
OB-3	8	0.209(4)	0.648(2)	0.068(3)	0.8	$\frac{1}{2}$
OB-4	8	0.319(3)	0.362(2)	0.060(3)	0.8	$\frac{1}{2}$
OB-5	8	0.435(3)	0.471(2)	0.089(3)	0.8	$\frac{1}{2}$
OB-6	8	0.553(3)	0.501(2)	0.072(3)	0.8	$\frac{1}{2}$
OB-7	8	0.665(3)	0.347(2)	0.069(3)	0.8	$\frac{1}{2}$
OB-8	8	0.769(4)	0.633(2)	0.074(3)	0.8	$\frac{1}{2}$
OB-9	8	0.891(3)	0.352(2)	0.085(3)	0.8	$\frac{1}{2}$
OS-1	4	0.123(3)	$\frac{3}{4}$	0.163(3)	0.8	
OS-2	4	0.238(3)	$\frac{1}{4}$	0.144(2)	0.8	
OS-3	4	0.352(3)	$\frac{3}{4}$	0.156(2)	0.8	
OS-4	4	0.526(3)	$\frac{1}{4}$	0.135(2)	0.8	
OS-5	4	0.655(3)	$\frac{3}{4}$	0.139(2)	0.8	
OS-6	4	0.772(3)	$\frac{1}{4}$	0.155(2)	0.8	
OS-7	4	0.890(3)	$\frac{3}{4}$	0.157(2)	0.8	
OS-8	4	1.011(2)	$\frac{1}{4}$	0.157(2)	0.8	
OC-1	8	0.194(2)	0.477(8)	0.261	0.8	
OC-2	8	0.317(2)	0.004(8)	0.249(2)	0.8	
OC-3	8	0.441(2)	0.485(8)	0.228(2)	0.8	
OC-4	8	0.568(2)	0.495(8)	0.240(2)	0.8	

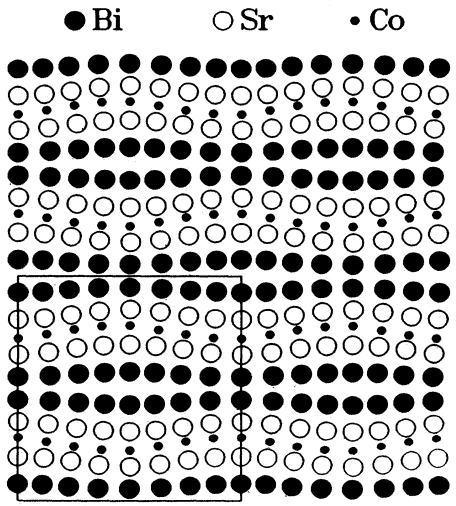

FIG. 2. Projection down the b axis of the positions of metal atoms. The origin is at the bottom left, with the x axis horizontal, and the z axis vertical. The solid line is the outline of the unit cell. Two periods are plotted along each direction. The Bi-Sr-Co-Sr-Bi slabs are displaced along z, and the amplitude of the displacement oscillates sinusoidally along x. The layers are also compressed and extended along x, as shown by the varying gap between the solid Bi circles.

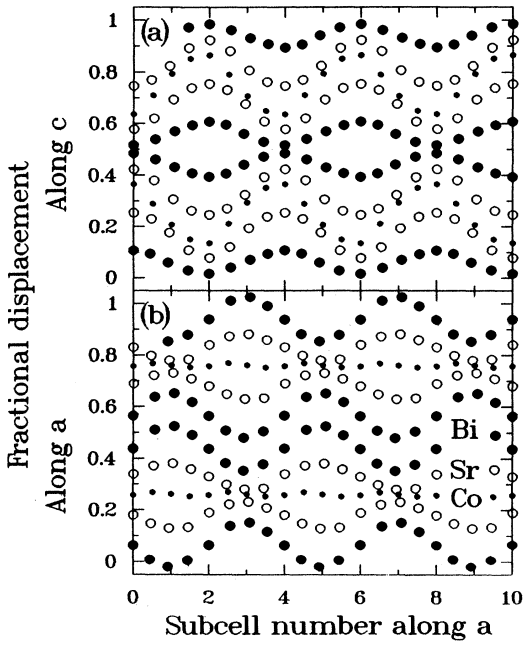

FIG. 3. The displacements of the atoms in the distortion of the structure. This figure should be compared to Fig. 2 of Ref. 6. The average vertical position of each row of atoms is the average z coordinate for that row. The displacements about this average are (a) four times the deviation of z from its average value, and (b) four times the deviation of x from its ideal values of 0,0.1,2, ... Since a and c are both about 22 Å, a deviation of 0.1 vertical unit in the figure corresponds to an atomic displacement of about 0.55 Å.

gen content corresponds to a Co valence greater than +2, again contrary to Ref. 8, which reported a Cu valence below +2 in 2:2:0:1 (Cu).

Figure 3(a) shows the displacement along z produced by the up-and-down flexing of the slabs. This flexing is almost purely sinusoidal with amplitude 0.5 and 0.3 Å for the Sr and Bi layers, respectively, but it is more distorted for the Co layer, with obvious components from higher harmonics. These harmonics stem from the displacement of Co atoms toward the regions of the Bi layers where the Bi is separated by oxygen in bridging positions (see below). In a simple ionic picture of Bi +3 and O −2 point ions, those regions are more negative than the other regions of the Bi-O layers, where the oxygens are in rocksalt positions, and they would be expected to attract positive Co ions.

Figure 3(b) shows the associated compression and extension of the slabs along the a axis. In the 2:3:0:1 (Fe) phase, the Sr at the center of the perovskite slab showed negligible compression, corresponding to a simple elastic model where the center of the slab is at the so-called neutral plane. Here, however, the Co atoms at the center of the plane show some compression. Again, this may be due to the negatively charged perovskite regions at the convex part of the slabs.

Figure 4(a) shows the ideal oxygen distribution for rocksalt and bridging types. The actual distribution [Fig. 4(b)] is disordered, and each oxygen site has 50% occupancy. The reason for this disorder is probably that, contrary to the exhibited by the 2:2:0:1 (Cu), 2:2:1:2 (Cu), and 2:3:0:2 (Fe) phases, the Bi atoms here do not form ribbons, but are equally spaced along the y axis. Therefore, more patterns of Bi-O bonds become possible, perhaps producing domains or perhaps producing true disorder. Nevertheless, the mechanism of oxygen insertion found in 2:3:0:2 (Fe) is clearly recognizable here, in spite of the disorder; the periodic alternation between the rocksalt and the perovskite types allows a ninth oxygen row to be inserted for every eight Bi rows.

To determine the evolution of the structural modulation upon increasing the doping content within the $Bi_2Sr_2Cu_{1-x}M_xO_y$ series, transmission-electron-microscopy studies were performed. Electron diffraction patterns obtained with a 0.27-μm selected-area aperture, looking down to the c axis, were collected for several samples and Fig. 5 displays the most representative ones. In order to keep a consistent set of axes throughout for easy comparison, the intense subcell reflections are indexed with the 5.4×5.4×25 Å F-centered orthorhombic subcell used for example in Ref. 16. In all cases, with the a translation of the subcell slightly shorter than b, the modulation occurs along a. On the $hk0$ section, the substructure allows only spots with h and k even due to the F centering of the lattice. In order to index the superstructure reflections, which are not the same in all cases, we used a second reference system denoted by asterisks. The extra spots due to the structure modulation along the a axis are labeled with h^*k0. For $Bi_2Sr_2CoO_y$ [pattern (d)], in agreement with the above x-ray single-crystal work the structural modulation is commensurate with multiplicity 4.

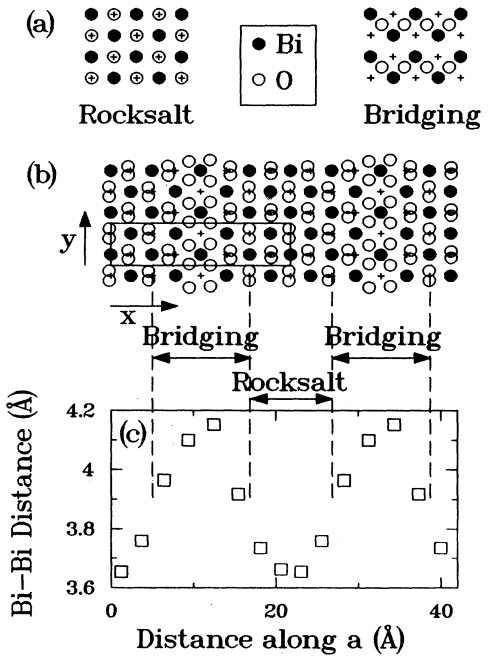

FIG. 4. (a) The two competing types of planar arrangement of oxygen atoms, designated here rocksalt and bridging. The plus signs indicate rocksalt positions throughout. (b) Section of the structure at $z=0.06$ through the Bi layer. Only half of the sites shown are occupied. The details of the local ordering of oxygen in occupying these sites is unknown, although clearly the two overlapping sites at a given rocksalt position cannot both be occupied simultaneously. Rocksalt- and bridging-type regions are indicated. The modulation allows the insertion of an extra oxygen atom every eight Bi rows. (c) Bi-Bi distances plotted with the same scale along x as in Fig. 3(b). With respect to the Bi-Bi distance of 3.86 Å in the substructure, the bridging-type region is expanded and the rocksalt-type region is compressed.

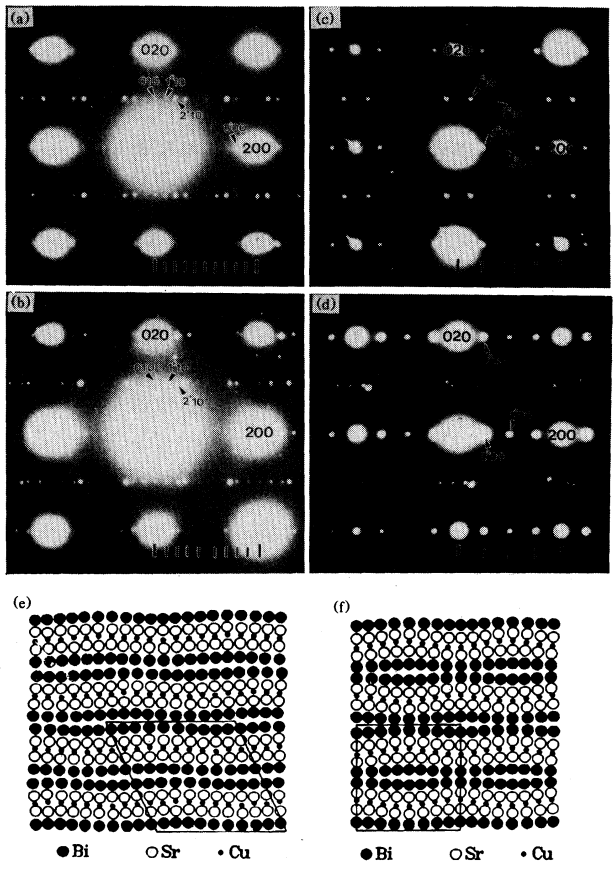

FIG. 5. Selected-area electron diffraction patterns for (a) $Bi_2Sr_2CuO_y$, (b) $Bi_2Sr_2Cu_{0.9}Fe_{0.1}O_y$, (c) $Bi_2Sr_2Cu_{0.6}Fe_{0.4}O_y$, and (d) $Bi_2Sr_2CoO_y$. The electron beam is along the c axis and a 0.27-μm selected-area aperature is used. The main diffractions of the tetragonal subcell with $a=b\cong 0.54$ nm are labeled with $hk0$, while the additional diffractions of the superstructure due to the structural modulation along the a axis are labeled h^*k0. Schematic drawing of the superstructures in the a-c plane are shown in (e) for $Bi_2Sr_2CuO_y$ (Ref. 8) and (f) for $Bi_2Sr_2CoO_y$ from this work.

For $Bi_2Sr_2CuO_y$ [pattern (a)], the structural modulation is still commensurate, but with multiplicity 5, in agreement with the work of Onoda and Soto.[8] For $Bi_2Sr_2Cu_{1-x}Fe_xO_y$ with $x=0.1$ and 0.4 [patterns (b) and (c), respectively], the structural modulation along the a axis is incommensurate.

A comparison of (a) and (d) reveals interesting features. In Fig. 5(a) for the pure Cu phase, there are nine modulation spots equally spaced between the (000) and (200) subcell reflections or between the (010) and (210) subcell reflections, indicating a commensurate modulation of multiplicity 5. On the other hand, Fig. 5(d) for the Co phase shows only three modulations spots equally spaced between the (000) and (200) subcell reflections and a few weak spots along (h10), possibly due to multiple reflections. This is consistent with the structure model established by x-ray diffraction shown in Fig. 5(f) for the Co phase, that the superstructure cell resulting from the a-axis modulation has a body-centered arrangement, allowing only reflections with the sum of indices even. The quasiabsence of reflections of the type (h^*10) for the Co phase (as compared to the Cu phase) is due to the b-glide absence of the $I2mb$ space group, but some weak multiple reflections are visible here. In other words, the lowering of the extended unit-cell symmetry in going from the Co to the Cu phase, i.e., from Figs. 5(f) to 5(e), allows more reflections, leading to the observed additional spots.

The $Bi_2Sr_2Cu_{1-x}Fe_xO_y$ series was also examined as a function of the Fe composition. We find that the electron diffraction patterns for low-Fe-content samples ($0<x<0.2$) [pattern (b) for example] are quite similar to that of the undoped phase $x=0$, suggesting that the superstructure is still monoclinic but with an incommensurate modulation of periodicity 4.65 ± 0.10. In contrast, the electron diffraction patterns for higher-Fe-content samples $0.3<x<0.5$ [pattern (c) for instance] bear a striking similarity to that of the pure Co phase, suggesting an orthorhombic superstructure, but the modulation is incommensurate with a periodicity of 4.3 ± 0.1 instead of 4. We noted that in Fig. 5(c), (h^*10) spots with h^*=odd

become clearly visible, an indication of the formation of ribbons in the Bi layer, which are ruled out by the *b* glide plane of the Co analog. In addition, there is a striking similarity between these two patterns. It is interesting to point out that the Fe ($x=0.5$) and full Co-doped phase have the same unit-cell volume and a similar modulation periodicity, and also note that the value of x at which the sharp drop in the subcell volume is observed also corresponds to the composition at which a drastic change in the modulation periodicity associated with a monoclinic-orthorhombic transition was found.

MAGNETISM

The superconducting properties of the Co- and Fe-doped $Bi_2Sr_2Cu_{1-x}M_xO_y$ samples were investigated using an ac mutual inductance apparatus. None of the doped samples were superconducting down to below 4.2 K in contrast to the undoped material which shows a T_c of 10 K.

The magnetic susceptibility measurements were performed for several members of the $Bi_2Sr_2Cu_{1-x}Co_xO_y$ series over the temperature range 4.2–300 K. At low Co concentrations, the temperature dependence was Curie type over the entire temperature range (data not shown). For $x=0.5$, a Curie temperature dependence is only obeyed above 100 K (Fig. 6), and at higher concentrations, the susceptibility develops a cusp, suggesting an antiferromagnetic ordering. With increasing Co content, the amplitude of this cusp increases and the temperature at which it occurs (T_N) shifts only slightly to lower temperature; for $Bi_2Sr_2CoO_y$ ($x=1$), $T_N=150$ K. Well above T_N, the susceptibility can be fit to a Curie-Weiss law of general formula $\chi_g=C_g(T+\Theta_p)+\chi_0$ where C_g, Θ_p, and χ_0 are the Curie constant, the paramagnetic Curie temperature, and the temperature-independent susceptibility, respectively (Fig. 7). Fits over the range of temperature 250–400 K and 300–400 K led, respectively, to the following parameters $\mu_{\text{eff}}=2.4\mu_B$, $\Theta_p=-130$ K, and a root-mean-square deviation from the Curie-Weiss law (sigma) of 0.2% and $\mu_{\text{eff}}=3.01\mu_B$, $\Theta_p=-78$, $\sigma=0.1\%$. Caution should be exercised in interpreting these results, as the lack of data above 400 K makes the values of μ_{eff} underestimated. If there is 2D behavior as in La_2CuO_4, where an upturn of the susceptibility (due to short-range antiferromagnetic order within the CuO_2 planes) was observed below 1000 K,[14] the values of Θ_p can be meaningless. In both cases, however, the values of $-\Theta_p$ are positive, indicating (within the range of temperature investigated) the presence of ferromagnetic interactions. The effective magnetic moment of $3.01\mu_B$ found for Co is smaller than that expected (3.9) for high-spin Co^{2+} ($S=\frac{3}{2}$) or (4.9) for Co^{3+} high-spin ($S=2$) and greater than that expected (1.7) for low-spin Co^{2+} ($S=\frac{1}{2}$) or (0) for low-spin Co^{3+} ($S=0$). Thus, the valence of Co cannot be simply determined from magnetic measurements.

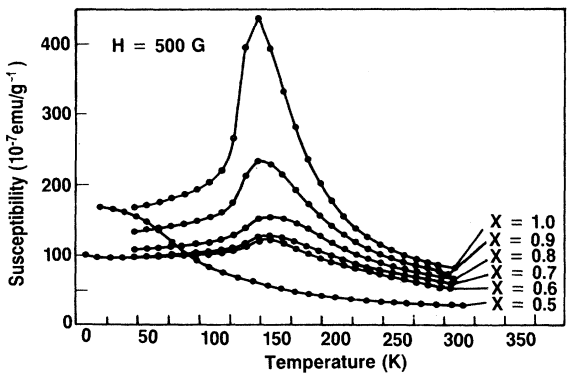

FIG. 6. Temperature dependence of the susceptibility for several members of the $Bi_2Sr_2Cu_{1-x}Co_xO_y$ series. The data were collected on warming the samples in a field of 500 G.

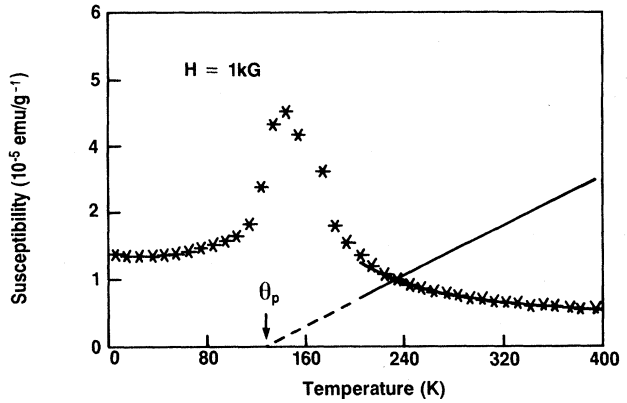

FIG. 7. The variation of the susceptibility from 4.2 to 400 K in a field of 1 kG is shown for a $Bi_2Sr_2CoO_y$ sample. Crosses refer to the data points. The solid line is a fit of the data to a Curie-Weiss law with the parameters given in the text. Also shown is the $1/\chi$ vs temperature plot from which the effective magnetic momentum per Co atom and the paramagnetic Curie temperature, reported in the text, were deduced.

Magnetic transitions are usually sensitive to changes in compositions, which can be caused by changes in processing. This is also true for the $Bi_2Sr_2CoO_y$ phase. A sample processed in air at $T=890\,^\circ$C (denoted *A*) has a T_N of 150 K, and by lowering the annealing temperature of the sample in air to 840 °C, we found that T_N moves to higher temperatures (up to 270 K). This ordering temperature decreases to 100 K when the compound is treated at 800 °C under argon (Fig. 8). When such a sample is annealed under oxygen, as reported in the experimental section, another phase forms that has no magnetic order so that the magnetic transition vanishes (Fig. 8). Such a large dependence of the magnetic ordering temperature on stoichiometry also occurs for other perovskites, such as La_2CuO_4,[17–19] La_2NiO_4,[20] or $YBa_2Cu_3O_6$.[21–23] For both La_2CuO_4 and $YBa_2Cu_3O_6$, however, T_N is shifted to lower temperatures with increasing oxygen content, the opposite of what we observe here. We also found that the antiferromagnetic ordering temperature in $Bi_2Sr_2CoO_y$ is lowered if the materials are made with cobalt deficiency, indicating again that there is a close correlation between composition and magnetic properties for this compound.

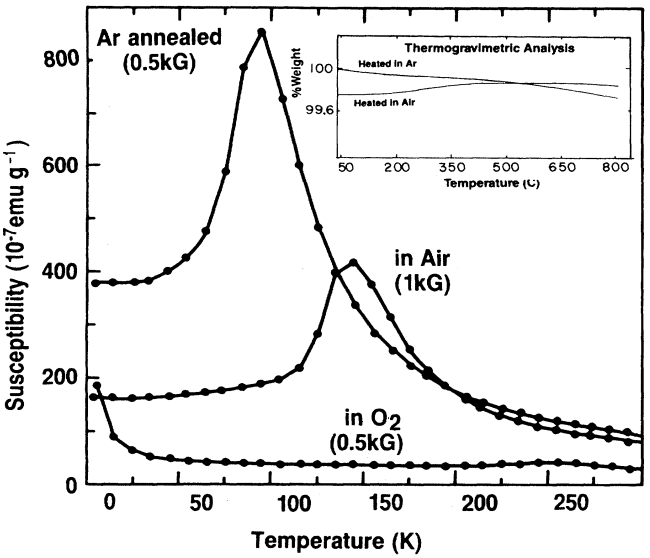

FIG. 8. The dependence of the antiferromagnetic ordering temperature upon ambient is shown for the $Bi_2Sr_2CoO_y$ phase. The measurements were performed on warming the samples. The inset shows a TGA trace for a sample heated in argon, cooled in argon, and then reheated in air. A change of 0.06 oxygen atoms per unit formula was estimated between air and argon annealed samples.

Magnetization as a function of applied field (up to 5 T) has been measured on several samples. Figure 9 shows the results for a pellet at several temperatures below T_N. In contrast to the linear field dependence expected for a normal antiferromagnet, we observe at $T=200$ K a change in curvature and an inflection point at 3 ± 0.5 T (without hysteresis). As the temperature decreases, this sudden increase in magnetization is smeared and shifted to higher fields, and hysteresis develops. This is reminiscent of a metamagnetic state or hidden ferromagnetism as has been recently reported for La_2CuO_4.[24]

Two oriented crystals were investigated for magnetism with identical results. Figure 10 shows the susceptibility (uncorrected for demagnetization) for several rectangularlike crystals (of overall weight 2.6 mg and of overall dimensions $4\times1\times0.1$ mm^3), with the applied field parallel to the *a*, *b*, and *c* crystallographic directions. When the applied field is parallel to *a*, clear evidence for antiferromagnetism is observed at $T_N=150$ K. But, in addition a well-defined peak of lower amplitude [which is barely detectable when the measurements are performed on bulk (see, for instance, inset of Fig. 9)] shows up at $T=100$ K. This peak may be either due to impurities or is intrinsic to the compound. For instance, two magnetic transitions were found within the layered La_2CoO_4.[25] Experiments are in progress to determine the origin of this peak, and we will not comment any further. However, a rather striking feature of Fig. 10 is the large difference in the amplitude of the susceptibility both above and below T_N, depending on the orientation of the applied field. Such a large difference most likely arises from a large crystalline anisotropy, as expected from the structure. When the applied field is parallel to *c*, the susceptibility above and below T_N does not change significantly, indicating that it is difficult to move the spins out of the planes, and already defining the orientation of the spins (within the *ab* plane). The large anisotropy of the susceptibility above T_N ($\chi_{400}\|\mathbf{a}$ and $\chi_{400}\|\mathbf{b} > \chi_{400}\|\mathbf{c}$) is also suggestive that $Bi_2Sr_2CoO_y$ may be an Ising or *XY* antiferromagnet. This anisotropy in the susceptibility, where the field along *c* gives the smallest signal, is opposite to that found by Thio

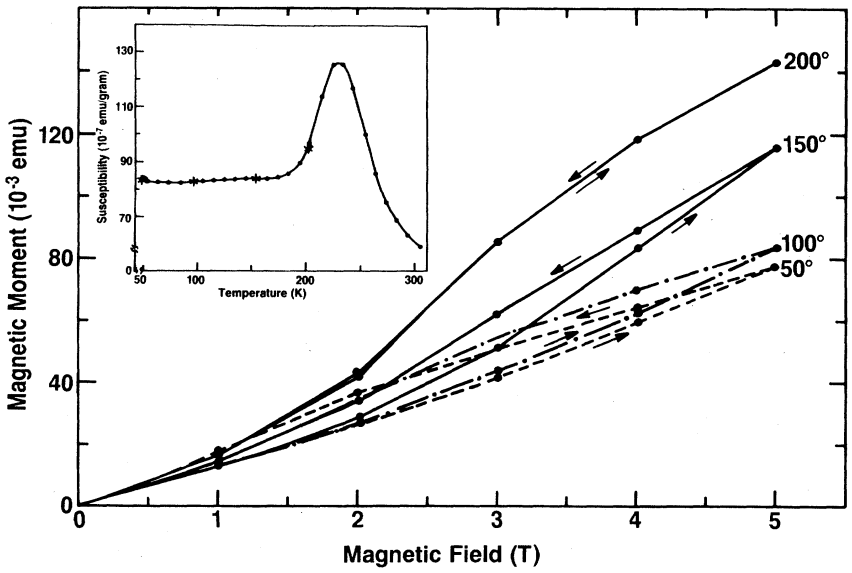

FIG. 9. Isothermal magnetization vs magnetic field for applied fields up to 5 T. The arrows indicate whether the measurements were taken on cooling or in warming the sample. Note clearly for the data taken at 200 K the appearance of a field induced transition without hysteresis. The inset shows the susceptibility temperature dependence for the same sample.

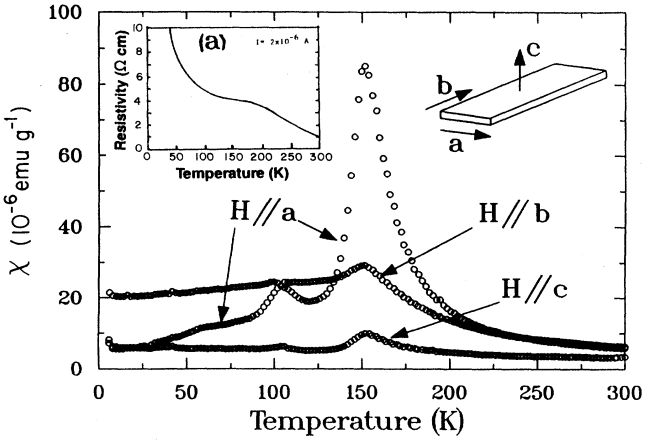

FIG. 10. Susceptibility as a function of temperature in single crystals of $Bi_2Sr_2CoO_6$ (see text) with in the right corner of the figure the way that the measurements were done with the applied field either parallel or perpendicular to the c axis. Inset (a) shows the resistivity measurements performed on a lamellar-like aggregate (see text) along the long direction.

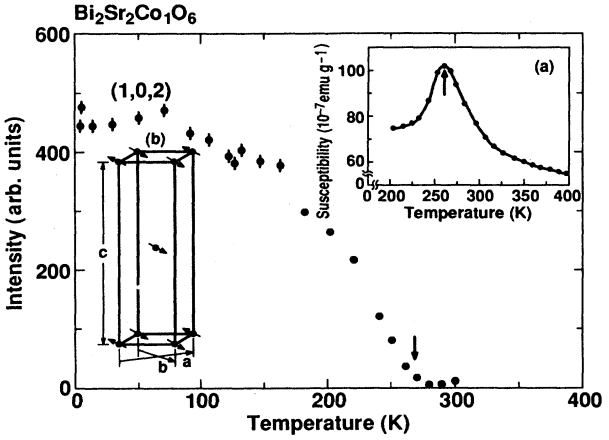

FIG. 11. Temperature dependence of the (1,0,2) integrated intensity showing the magnetic ordering at $T=270$ K for the $Bi_2Sr_2CoO_y$ phase. Inset (a) shows the susceptibility temperature dependence for the same sample. Inset (b) shows the spin structure.

et al.[24] on La_2CuO_4 (in their crystal, a field parallel to b is equivalent to a field parallel to c in our crystal). Resistivity measurements on a $Bi_2Sr_2CoO_y$ lamellarlike aggregate (consisting of several plateletlike crystals) from the same batch as used for magnetic measurements is shown in Fig. 10(a). The resistivity increases with decreasing temperature indicative of a semiconducting or insulating regime. Note a change in the rate at which the resistivity increases at $T=180\pm10$ K. It is interesting to note that it is over the same temperature range that a magnetic transition is observed suggesting that both are related. We should point out that similar measurements made on sintered pellets gave greater values for the resistivity at room temperature (on the order of 20 Ω cm instead of 1 for the crystal), and also no anomalies in the temperature-dependence resistivity curve were observed, even though the same sample shows a magnetic transition. Such differences may be due to grain boundaries and/or inhomogeneities problems, always greater in bulk than in crystals.

To further investigate the magnetic anomaly observed in the susceptibility, neutron diffraction was performed on a powder sample. This sample was prepared in air at 840 °C in contrast to 890 °C for the previous sample denoted A, thus explaining the difference in T_N between both samples. Here we briefly present some of the results; more details will be published elsewhere.[26] Various antiferromagnetic reflections of the type $10L$ were observed at low temperature. This cell indexing refers to the subcell of dimensions $5.459\times5.462\times23.45$ Å^3, where the a axis is one-quarter of that in the modulated structure. Figure 11 shows the temperature dependence of the (102) magnetic peak which exhibits a Néel temperature of $T_N=270$ K, in agreement with the susceptibility (measured on the same sample) shown in the inset. The intensity does not fall abruptly to zero at T_N. This smearing of T_N may be due to critical scattering or to inhomogeneities in the sample, because, as already noted, T_N is sensitive to composition changes. From the observed magnetic intensities, the spin structure (Fig. 11, inset) has spins lying in the plane perpendicular to c, in agreement with the susceptibility data. The spins point perpendicular to the direction of the antiferromagnetic wave vector, τ, which is along either the a or b axis. The difference between a and b cannot be resolved directly from the subcell peaks due to the near tetragonality of the substructure. However, because of the structural modulation, we also observe superlattice reflections which are purely magnetic in character. From these, we can conclude[26] that the spins point along the b axis, perpendicular to the structural modulation direction.

We have also studied the magnetic properties of $Bi_2Sr_2Cu_{1-x}Fe_xO_y$, which turns out to be simpler than for the Co series. For the undoped material the susceptibility is temperature independent. As Cu is replaced by Fe a Curie-Weiss behavior develops. No anomalies are observed in the curves of χ vs T [Fig. 12(a)], suggesting that there are no magnetic transitions. Over the range of temperature 200–350 K the data can be successfully fitted to a Curie-Weiss law as described above, giving an effective magnetic moment $\mu_{\text{eff}}=5.13\mu_B$ per Fe atom.

From this moment, it is again impossible to unambiguously ascribe a valence to Fe. Thus, the Fe Mössbauer effect was used to study the electronic valence state of Fe and the local structure in $Bi_2Sr_2Cu_{0.5}Fe_{0.5}O_y$. The Fe Mössbauer absorption spectrum was obtained in a standard transition geometry with a conventional constant acceleration spectrometer using a Co in Rh source. The room-temperature Mössbauer spectrum is shown in Fig. 12(b). The spectrum shows four resonance lines due to two nonequal quadrupole interactions, indicating that the iron ions are in two inequivalent sites (denoted as Fe_1 and Fe_2). The intensity of the two different quadrupole lines are in the ratio 4:3. The lines are broad (full width at half maximum equal to 0.50 mm/s), indicating a random distribution between Fe and Cu in the same crystallographic sites. The values of the quadrupole splittings are 1.64 and

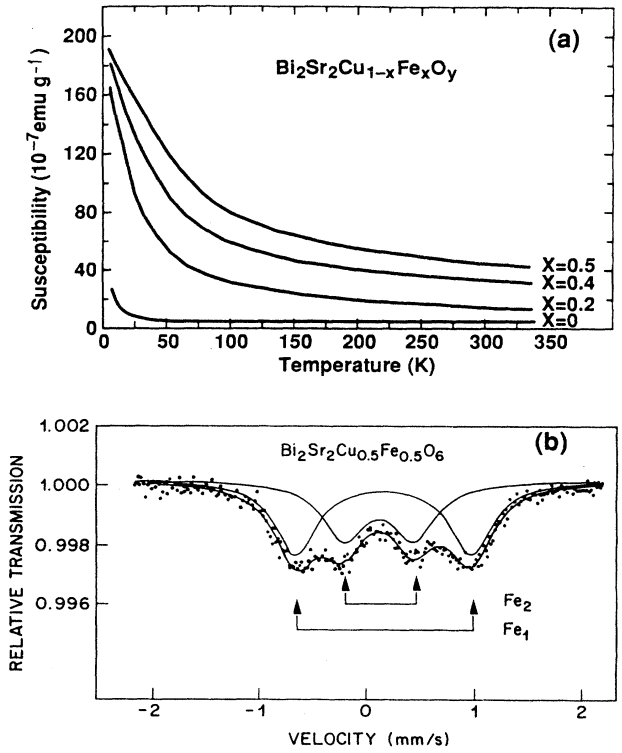

FIG. 12. The temperature-dependent susceptibility (collected in a field of 10 kG) for several samples of the $Bi_2Sr_2Cu_{1-x}Fe_xO_y$ series are shown in (a). In (b) the room-temperature Mössbauer absorption spectra of $Bi_2Sr_2Cu_{0.5}Fe_{0.5}O_y$ is displayed. Note the clear evidence for two quadrupole splittings.

0.65 mm/s for Fe_1 and Fe_2, respectively. The corresponding observed isomer shifts are 0.22 and 0.18 mm/s, indicating that iron is in the Fe^{3+} valence state.

DISCUSSION

This study of the $Bi_2Sr_2Cu_{1-x}M_xO_y$ system has shown that there is a subtle and delicate balance between composition, structural, and physical properties. The transport and magnetic properties of these materials are determined by the electronic state of each element in the material. In chemical terms, these properties are determined by the valence or oxidation state and spin state of each element and the nature of the bonding, ionic or covalent; in physical terms, they are determined by the nature of the wave function at the Fermi level (the degree of hybridization of the 3*d* metal orbitals with oxygen 2*p* levels, for example). The following discussion addresses these properties. In some oxides, bismuth can adopt either the valence 3+ or 5+ or both, as the result of the hybridization of the Bi 6*s* and O 2*p* levels. This possibility is ruled out here, since x-ray photoemission measurements on the Bi cuprate phases, either undoped or doped with Co or Fe, have shown that Bi is only +3 in these phases.[27] In agreement with these measurements, band-structure calculations[28] show that the Bi 6*s* band is well below the Fermi level and the Bi 6*p* band well above, thereby implying Bi^{3+}. Furthermore, the Bi-O stereochemistry from the crystal studies does not correspond to Bi^{5+}.

The subcell of the new $Bi_2Sr_2CoO_y$ compound is isostructural to that of the 10-K phase. Both compounds contain MO_2 layers with elongated CuO_6 or CoO_6 octahedra and crystallographically sheared Bi-O layers. The full structure, however, differs because the periodicity of the structural modulation is four subcells for Co and five for Cu. The structural modulation in $Bi_2Sr_2CoO_y$ is caused by the insertion of one extra row of oxygen atoms for every eight rows of Bi atoms, as in $Bi_2Sr_3Fe_2O_y$, where one extra row of oxygen is inserted in every ten rows of Bi. As a result, the oxygen content for $Bi_2Sr_2CoO_y$, which would be 24 if the Bi slabs were 100% rocksalt structure, is increased to 25, or one extra oxygen for every four Co atoms. A simple valence count (assuming Bi^{3+} and Sr^{2+}) gives the formal valence of Co as 2.50 (50% of Co^{2+} and 50% of Co^{3+}). Within the Cu phase where the structural modulation is five, there should be (according to our model[6]) an extra oxygen for every five Cu atoms, leading to a formal valence of Cu of 2.4, compared to 2.2 obtained from chemical analysis.[4] In $Bi_2Sr_2CuO_y$, the Cu 3*d* levels mix with oxygen 2*p* levels so that the electrons collectively give rise to both metallic behavior and to temperature-independent susceptibility [Fig. 12(a)]. In moving to the left of Cu in the Periodic Table, the energy difference between the metal 3*d* levels and oxygen 2*p* levels increases so that the orbital overlap decreases, resulting in a localization of the *d*-like electrons and producing an insulator. This applies to the $Bi_2Sr_2CoO_y$ phase (Co left of Cu in the Periodic Table), since both insulating and paramagnetic behavior are observed. However, Co has a mixed valence, and in a localized electron regime, one normally expects two different sites or environments for Co, as in Co_3O_4. It is suggestive that for two of the four Co in the structure of $Bi_2Sr_2CoO_y$ (Co-1 and Co-4 in Table III), the Co is shifted toward one of the two apical oxygens on the distorted CoO_6 octahedron, so that this Co-O distance is almost as short as the four Co-O distances to the four equatorial oxygens. Thus, two of the Co atoms are nearly fivefold coordinated, while the other two are fourfold coordinated, indicating that two different sites for Co exist within the structure. (Two different sites are also seen in the Mössbauer results for the $Bi_2Sr_2Cu_{0.5}Fe_{0.5}O_y$ compound.) Thus, with two structural Co sites, the insulating behavior of $Bi_2Sr_2CoO_y$ in which Co has the formal valence 2.5 is not so surprising. In this compound, a formal valence of Co below +3 is also consistent with the fact that $Bi_2Sr_2CoO_y$ must be synthesized in a reducing atmosphere, not an oxidizing one. A reducing atmosphere might be expected to favor Co^{2+} whereas an oxidizing atmosphere stabilizes the $n=2$ phase, in which, by analogy to the Fe compound, the valence of Co is probably +3.

Now we consider the lattice parameters for the Fe- and Co-doped $Bi_2Sr_2Cu_{1-x}M_xO_y$ series. In both series, the unit-cell volume does not change continuously, but drops sharply from 705 to 699 Å^3, at $x=0.25$ for Fe and $x=0.5$ for Co. Lattice instabilities or changes in the electronic state or spin configuration of the 3*d* metal ions generally account for such sharp changes in unit-cell volume. For

instance, increasing the oxidation state of an ion or changing its spin configuration from high spin (HS) to low spin (LS) reduces its ionic radius and thereby the unit-cell volume of the compound containing this ion. On the other hand, sudden changes in the electronic state of the $3d$ metal ions should produce equally drastic changes in the effective magnetic moment per $3d$ metal ion, and such changes in the moment per Co or Fe were not observed for either the Co or Fe series. It is more likely, therefore, that lattice instabilities cause the sharp drops in Fig. 1. These instabilities may simply be related to the observed structural change (monoclinic-orthorhombic) associated with the sudden change in the periodicity of the structural modulation from 5 to 4 observed in going from the Cu to the Co system, thereby suggesting a noncontinuous change of the modulation. Among the Bi compounds, the structural modulation determines the oxygen content and thereby the valence of the $3d$ metal. Moreover, we have shown that Fe enters the structure as a $+3$ ion whereas Co has an average valence of 2.5 in the fully-doped compound. Thus if the structural modulation occurs at some specific valence of M, it should occur at a value of x half as large in the Fe series as in the Co series, as observed.

We turn now to the magnetism in $Bi_2Sr_2CoO_y$. We found for this phase a 3D antiferromagnetic transition which, depending on the stoichiometry and processing of the samples, occurs over a range of temperature from 100–280 K. Within the CoO_2 planes, the CoO_6 elongated octahedra share corners, so that superexchange Co-O-Co interactions rather than direct Co-Co exchange interactions probably determine the magnetic interactions. Thus, one would expect the magnetic transition to be sensitive to stoichiometry of oxygen or cobalt, as we observe experimentally.

The sharpness of the susceptibility peak at the Néel temperature is suggestive of a ferromagnetic component among the magnetic interactions. This is also supported by the field-dependent magnetization curves collected at constant temperature below T_N which show a step at a critical field denoted H_c. For applied fields greater than H_c and up to 5 T we did not reach a saturation in magnetization. A similar behavior was observed for La_2CuO_4.[24] It was ascribed to a flip of the small component of the Cu spins normal to the CuO_2 layers.[29–31] However, the peak in susceptibility was seen for fields normal to the plane, whereas here it is largest for fields in the plane, suggesting that the canted component of the spins lies in the plane in our case. A comparison of the field-induced magnetization data for La_2CuO_4 (see figure in Ref. 24) with that of Fig. 9 for $Bi_2Sr_2CoO_y$ indicates that in both materials the field-induced antiferromagnetic-ferromagnetic (AF-F) transition occurs at the same field (3–4 T), and that the amplitude of this transition when reported in μ_B per Co atom is of the same order, leading to the belief that the energy required for the transition is similar in both materials. For La the canting is out of the plane in contrast to in the plane with Bi phase (i.e., for La the AF-F transition involves a reorientation of a small ferromagnetic moment in alternate sheets, whereas in the Bi compound according to our results it involves a reorientation of a small ferromagnetic moment within the CoO_2 layer). Usually one expects the interlayer coupling to be much weaker than the intralayer coupling. Our results do not seem to support this point. At present we cannot qualitatively explain such a difference which may be related to the canting transition (i.e., symmetry of the spin system) which is more complicated, due to the structural modulation, for the Co phase than for the La_2CuO_4 compound. Also, it turns out that there are four different Co atoms in the superstructure, and perhaps not all of them are canted in the same way.

In addition to this metamagnetic behavior, the elastic neutron-scattering data shows that the spin structure of $Bi_2Sr_2CoO_y$ is similar to La_2CuO_4, since the antiferromagnetic wave vector and the spin direction are perpendicular, with the spins pointing along the b axis. Alternatively, the anisotropy in the susceptibility above T_N suggests XY or Ising behavior as in La_2CoO_4. Thus, further neutron-scattering experiments on single crystals would be useful to look for 2D correlations above T_N and to study the inelasticity of the scattering.

In summary, we have reported the synthesis of new Bi-based phases $Bi_2Sr_2Cu_{1-x}M_xO_y$ (M=Fe, Co) which have similar structure to the 10-K superconducting $Bi_2Sr_2CuO_y$ phase. The substitution of Cu by Co reduces the structure modulation (caused by the uptake of an oxygen atom every ten or eight Bi rows) from 5 to 4. But based on the study of Fe and Co solid solutions, it appears that this structural transition is discontinuous. This might account for the difficulties encountered in removing oxygen from these materials. The fully doped Co material ($Bi_2Sr_2CoO_y$) is an antiferromagnetic insulator with a Néel temperature sensitive to deviation from stoichiometry and with a magnetic phase transition suggesting Ising critical behavior. However, further work remains to be done in order to determine the origin of the metamagnetic state in this compound and to better understand the role of the structural modulation on the magnetic properties.

ACKNOWLEDGMENTS

We wish to thank B. G. Bagley, V. J. Emery, M. Kastner, P. L. Key, R. Ramesh, J. M. Rowell, M. Whangbo, and J. H. Wernick for helpful discussions.

[1] J. M. Tarascon, L. H. Greene, P. Barboux, W. R. McKinnon, G. W. Hull, T. P. Orlando, K. A. Delin, S. Foner, and E. J. McNiff, Phys. Rev. B **36**, 8393 (1987).

[2] J. M. Tarascon, P. Barboux, P. F. Miceli, L. H. Greene, and G. W. Hull, Phys. Rev. B **37**, 4758 (1988).

[3] G. Xiao, F. H. Streitz, A. Gavrin, Y. W. Du, and C. L. Chien, Phys. Rev. B **35**, 8782 (1987).

[4] J. M. Tarascon, W. R. McKinnon, P. Barboux, D. M. Hwang, B. G. Bagley, L. H. Greene, G. W. Hull, Y. Le Page, N. Stoffel, and M. Giroud, Phys. Rev. B **38**, 8885 (1988).

[5]J. M. Tarascon, Y. Le Page, P. Barboux, B. G. Bagley, L. H. Greene, W. R. McKinnon, G. W. Hull, M. Giroud, and D. M. Hwang, Phys. Rev. B **37**, 9382 (1988).
[6]Y. Le Page, W. R. McKinnon, J. M. Tarascon, and P. Barboux (unpublished).
[7]C. C. Torardi, M. A. Subramanian, J. C. Calabrese, J. Gopalakrishnan, E. M. McCarron, K. J. Morrissey, T. R. Askew, R. B. Flippen, U. Chowdhry, and A. W. Sleight, Phys. Rev. B **38**, 225 (1989).
[8]M. Onoda and M. Soto, Solid Commun. **67**, 799 (1988).
[9]J. M. Tarascon, P. Barboux, G. W. Hull, R. Ramesh, L. H. Greene, M. Giroud, M. S. Hedge, and W. R. McKinnon, Phys. Rev. B **39**, 4316 (1989).
[10]J. M. Tarascon *et al.* (unpublished).
[11]J. M. Tarascon, W. R. McKinnon, L. H. Greene, G. W. Hull, and E. M. Vogel, Phys. Rev. B **36**, 226 (1987).
[12]G. Demazeau (private communication).
[13]E. M. Vogel, G. W. Hull, and J. M. Tarascon, Mater. Lett. **6**, 269 (1988).
[14]D. C. Johnston, S. K. Sinha, A. J. Jacobson, and J. M. Newson, Physica C **153–155**, 572 (1988).
[15]Y. Gao, P. Lee. P. Coppens, M. A. Subramanian, and A. W. Sleight, Science **241**, 954 (1988).
[16]S. A. Sunshine *et al.*, Phys. Rev. B **38**, 893 (1988).
[17]R. L. Greene, H. Maletta, T. S. Plaskett, J. G. Bednorz, and K. A. Muller, Solid State Commun. **63**, 379 (1987).
[18]D. C. Johnston, J. P. Stokes, D. P. Goshorn, and J. T. Lewandowski, Phys. Rev. B **36**, 4007 (1987).
[19]D. Vaknin, S. K. Sinha, D. E. Moncton, D. C. Johnston, J. M. Newsom, C. R. Safinya, and H. E. King, Jr., Phys. Rev. Lett. **58**, 2802 (1987).
[20]G. Aeppli and D. Buttrey, Phys. Rev. Lett. **61**, 203 (1988).
[21]J. M. Tranquada, D. E. Cox, W. Kunnmann, H. Mouden, G. Shirane, M. Suenaga, P. Zolliker, D. Vaknin, S. K. Sinha, M. S. Alvarez, A. J. Jacobson, and D. C. Johnston, Phys. Rev. Lett. **60**, 156 (1988).
[22]J. M. Tranquada, A. H. Moudden, A. I. Goldman, P. Zolliker, D. E. Cox, G. Shirane, S. K. Sinha, D. Vaknin, D. C. Johnston, M. S. Alvarez, and A. J. Jacobson, Phys. Rev. B **38**, 2477 (1988).
[23]P. F. Miceli, J. M. Tarascon, L. H. Greene, P. Barboux, M. Giroud, D. A. Neumann, J. J. Rhyne, L. F. Schneemeyer, and J. V. Waszczak, Phys. Rev. B **38**, 9209 (1988).
[24]Tineke Thio *et al.*, Phys. Rev B **38**, 905 (1988).
[25]K. Yamada *et al.*, Phys. Rev. **39**, 2336 (1989).
[26]P. Miceli *et al.* (unpublished).
[27]M. S. Hedge, C. C. Chang, T. Venkatesan, N. G. Stoffel, J. M. Tarascon, P. Barboux, X. D. Wu, and A. Inam (unpublished).
[28]M. H. Whangbo *et al.* (unpublished).
[29]M. A. Kastner *et al.*, Phys. Rev. B **38**, 6636 (1988).
[30]A. Aharony *et al.*, Phys. Rev. Lett. **60**, 1330 (1988); R. J. Birgeneau, M. A. Kastner, and A. Aharony, Z. Phys. B **71**, 57 (1988).
[31]R. J. Birgeneau and G. Shirane, *Physical Properties of High Temperature Superconductors,* edited by D. M. Ginsberg (World Scientific, Singapore, 1989).
[32]Y. Le Page, P. S. White, and E. J. Gabe, *Proceedings of the American Crystallographic Association Meeting, Program Abstracts Series 2* (ACA, New York, 1986), Vol. 14, Abstract PA 23, p. 24.
[33]E. J. Gabe, A. C. Larson, F. L. Lee, and Y. Le Page, *Crystallographic Computing 3: Data Collection, Structure Determination, Proteins and Databases,* edited by G. M. Sheldrick *et al.* (Oxford Univ. Press, New York, 1985), p. 167.

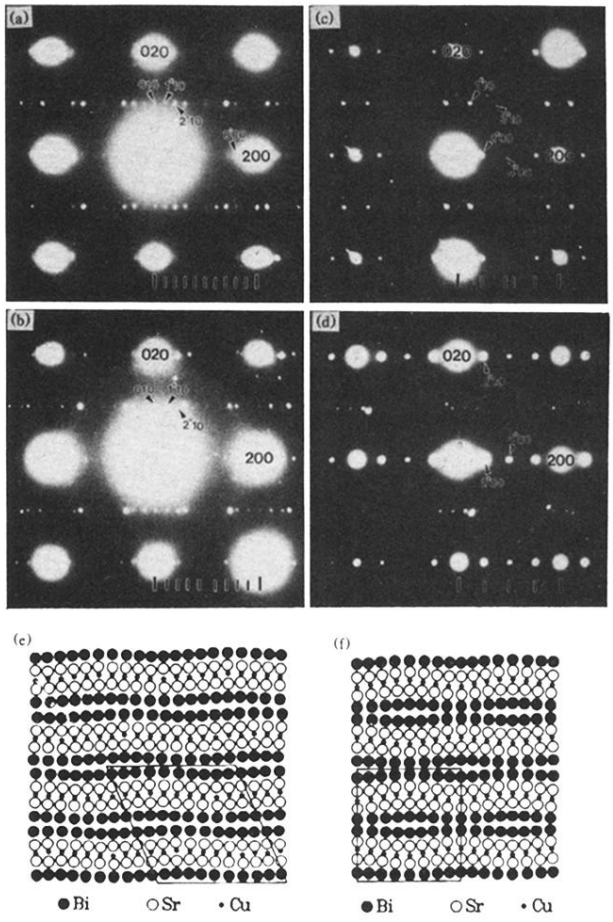

FIG. 5. Selected-area electron diffraction patterns for (a) $Bi_2Sr_2CuO_y$, (b) $Bi_2Sr_2Cu_{0.9}Fe_{0.1}O_y$, (c) $Bi_2Sr_2Cu_{0.6}Fe_{0.4}O_y$, and (d) $Bi_2Sr_2CoO_y$. The electron beam is along the c axis and a 0.27-μm selected-area aperature is used. The main diffractions of the tetragonal subcell with $a=b\cong 0.54$ nm are labeled with $hk0$, while the additional diffractions of the superstructure due to the structural modulation along the a axis are labeled h^*k0. Schematic drawing of the superstructures in the a-c plane are shown in (e) for $Bi_2Sr_2CuO_y$ (Ref. 8) and (f) for $Bi_2Sr_2CoO_y$ from this work.